REPORT DOCUMENTATION PAGE

Form Approved
OMB NO. 0704-0188

1. AGENCY USE ONLY (Leave Blank)	2. REPORT DATE 12/15/2008	3. REPORT TYPE AND DATES COVERED Final Progress Report Period 1/20/2004 – 4/19/2007

4. TITLE AND SUBTITLE
Atom Interferometry on Atom Chips-A Novel Approach Towards Precision Inertial Navigation Systems (PINS)

5. FUNDING NUMBERS
W911NF0410032
P

6. AUTHOR(S)
Wolfgang Ketterle, Vladan Vuletic, Mara Prentiss

7. PERFORMING ORGANIZATION NAME(S) AND ADDRESS(ES)
MIT 77 Mass Ave, Cambridge MA 02139
Harvard University, Cambridge, MA 02138

8. PERFORMING ORGANIZATION REPORT NUMBER

9. SPONSORING / MONITORING AGENCY NAME(S) AND ADDRESS(ES)
U. S. Army Research Office
P.O. Box 12211
Research Triangle Park, NC 27709-2211

10. SPONSORING / MONITORING AGENCY REPORT NUMBER

11. SUPPLEMENTARY NOTES
The views, opinions and/or findings contained in this report are those of the author(s) and should not be construed as an official Department of the Army position, policy or decision, unless so designated by other documentation.

12 a. DISTRIBUTION / AVAILABILITY STATEMENT
Approved for public release; distribution unlimited.

12 b. DISTRIBUTION CODE
.

1. ABSTRACT (Maximum 200 words)

Considerable progress was made during the grant period toward establishing a chip based atom interferometer. At the beginning of the gBECi period, no coherent on-chip beam splitter had been demonstrated. During the funding period, we developed two area enclosing interferometers with demonstrated coherence preservation: one using optical pulses, the other one using RF dressed potentials. Technical improvements in the moving guide technique should provide a $1cm^2$ enclosed area in a device with a length ~ 1 cm.
We addressed in several studies the role of interactions in a Bose-Einstein condensate. This can lead to phase diffusion and phase fluctuations. We showed that a BEC interferometer can be robust against phase fluctuations, that interactions can lead to number squeezing, which slows down phase diffusion, and led to a considerable enhancement of the coherence time, and finally, that soliton-type excitations in an interacting condensate can be used to read out the phase of the interferometer after recombining the split condensate Technical breakthroughs include improved atom chip fabrication methods, and continuous non-destructive optical readout of the interferometer phase.
In related work, we demonstrated quantum reflection with normal incidence and studied it for different surfaces. Single photon sources have been developed.

14. SUBJECT TERMS	15. NUMBER OF PAGES
	16. PRICE CODE

17. SECURITY CLASSIFICATION OR REPORT	18. SECURITY CLASSIFICATION ON THIS PAGE	19. SECURITY CLASSIFICATION OF ABSTRACT	20. LIMITATION OF ABSTRACT
UNCLASSIFIED	**UNCLASSIFIED**	**UNCLASSIFIED**	**UL**

NSN 7540-01-280-5500

Standard Form 298 (Rev.2-89)
Prescribed by ANSI Std. 239-18
298-102

Enclosure 1

GENERAL INSTRUCTIONS FOR COMPLETING SF 298

The Report Documentation Page (RDP) is used for announcing and cataloging reports. It is important that this information be consistent with the rest of the report, particularly the cover and title page. Instructions for filling in each block of the form follow. It is important to ***stay within the lines*** to meet ***optical scanning requirements.***

Block 1. Agency Use Only (Leave blank)

Block 2. Report Date. Full publication date including day, month, and year, if available (e.g. 1 Jan 88). Must cite at least year.

Block 3. Type of Report and Dates Covered. State whether report is interim, final, etc. If applicable enter inclusive report dates (e.g. 10 Jun 87 - 30 Jun 88).

Block 4. Title and Subtitle. A title is taken from the part of the report that provides the most meaningful and complete information. When a report is prepared in more than one volume, repeat the primary title, and volume number, and include subtitle for the specific volume. On classified documents enter the title classification in parentheses.

Block 5. Funding Numbers. To include contract and grant numbers; may include program element number(s) project number(s), task number(s), and work unit number(s). Use the following labels:

C - Contract	**PR** - Project
G - Grant	**TA** - Task
PE - Program Element	**WU** - Work Unit Accession No.

Block 6. Author(s). Name(s) of person(s) responsible for writing the report, performing the research, or credited with the content of the report. If editor or compiler, this should follow the name(s).

Block 7. Performing Organization Name(s) and Address(es). Self-explanatory.

Block 8. Performing Organization Report Number. Enter the unique alphanumeric report number(s) assigned by the organization performing the report.

Block 9. Sponsoring/Monitoring Agency Name(s) and Address(es) Self-explanatory.

Block 10. Sponsoring/Monitoring Agency Report Number. (*if known)*

Block 11. Supplementary Notes. Enter information not included elsewhere such as; prepared in cooperation with....; Trans. of...; To be published in.... When a report is revised, include a statement whether the new report supersedes or supplements the older report.

Block 12a. Distribution/Availability Statement. Denotes public availability or limitations. Cite any availability to the public. Enter additional limitations or special markings in all capitals (e.g. NORFORN, REL, ITAR).

- **DOD** - See DoDD 4230.25, "Distribution Statements on Technical Documents."
- **DOE** - See authorities.
- **NASA** - See Handbook NHB 2200.2.
- **NTIS** - Leave blank.

Block 12b. Distribution Code.

- **DOD** - Leave Blank
- **DOE** - Enter DOE distribution categories from the Standard Distribution for unclassified Scientific and Technical Reports
- **NASA** - Leave Blank.
- **NTIS** - Leave Blank.

Block 13. Abstract. Include a brief (*Maximum 200 words)* factual summary of the most significant information contained in the report.

Block 14. Subject Terms. Keywords or phrases identifying major subject in the report.

Block 15. Number of Pages. Enter the total number of pages.

Block 16. Price Code. Enter appropriate price code (NTIS *only*).

Block 17. - 19. Security Classifications. Self-explanatory. Enter U.S. Security Regulations (i.e., UNCLASSIFIED). If form contains classified information, stamp classification on the top and bottom of the page.

Block 20. Limitation of Abstract. This block must be completed to assign a limitation to the abstract. Enter either UL (Unlimited) or SAR (same as report). An entry in this block is necessary if the abstract is to be limited. If blank, the abstract is assumed to be unlimited.

REPORT DOCUMENTATION PAGE (SF298)
(Continuation Sheet)

b. "The Report Documentation Page (SF298) Continuation Sheet (Enclosure 2)" or a plain piece of paper must include brief, but complete, information for each of the following categories:

(1) Submissions or publications under ARO sponsorship during this reporting period. List the title of each and give the total number for each of the following categories:

(a) Papers published in peer-reviewed journals

1. T.A. Pasquini, Y. Shin, C. Sanner, M. Saba, A. Schirotzek, D.E. Pritchard, and W. Ketterle, Quantum reflection of atoms from a solid surface at normal incidence, Phys. Rev. Lett. 93, 223201 (2004).
2. M. Saba, T.A. Pasquini, C. Sanner, Y. Shin, W. Ketterle, and D.E. Pritchard, Continuous measurement of the relative phase of two Bose-Einstein condensates using light scattering, Science 307 (2005).
3. Y. Shin, G.-B. Jo, M. Saba, T.A. Pasquini, W. Ketterle, and D.E. Pritchard, Optical Weak Link between Two Spatially Separate Bose-Einstein Condensates, Phys. Rev. Lett. 95, 170402 (2005).
4. Y. Shin, C. Sanner, G.-B. Jo, T.A. Pasquini, M. Saba, W. Ketterle, D.E. Pritchard, M. Vengalattore, and M. Prentiss, Interference of Bose-Einstein Condensates on an Atom Chip, Phys. Rev. A 72, 021604(R) (2005).
5. Vengalattore M, Prentiss M, Radial confinement of light in an ultracold anisotropic medium, Phys. Rev. Lett. ,95 , 243601 (2005)
6. A.T. Black, J. K. Thompson, and V. Vuletic, On-Demand Superradiant Conversion of Atomic Spin Gratings into Single Photons with High Efficiency., Phys. Rev. Lett. 95, 133601 (1-4) (2005).
7. T.A. Pasquini, M. Saba, G. Jo, Y. Shin, W. Ketterle, D.E. Pritchard, T.A. Savas, and N. Mulders, Low velocity quantum reflection of Bose-Einstein condensates, Phys. Rev. Lett. 97, 093201 (2006).
8. A High-Brightness Source of Narrowband, Identical-Photon Pairs. J. K. Thompson, J. Simon, H. Loh, and V. Vuletic, Science 303, 74-77 (2006).
9. I. Teper, Y. Lin, and V. Vuletic , Resonator-Aided Detection of Single Atoms on a Microchip, Phys. Rev. Lett. 97, 023002 (2006).
10. G.-B. Jo, Y. Shin, S. Will, T.A. Pasquini, M. Saba, W. Ketterle, D.E. Pritchard, M. Vengalattore, and M. Prentiss, Long Phase Coherence Time and Number Squeezing of two Bose-Einstein Condensates on an Atom Chip, Phys. Rev. Lett. 98, 030407 (2007).

11. C.A. Christensen, S. Will, M. Saba, G.-B. Jo, Y.Shin, W. Ketterle, and D.E. Pritchard, Trapping of Ultracold Atoms in a Hollow-core Photonic Crystal Fiber, Phys. Rev. A 78, 033429 (2008).
12. G.-B. Jo, J.-H. Choi, C.A. Christensen, T.A. Pasquini, Y.-R. Lee, W. Ketterle, and D.E. Pritchard, Phase Sensitive Recombination of Two Bose-Einstein Condensates on an Atom Chip, Phys. Rev. Lett. 98, 180401 (2007).
13. J. Simon, H. Tanji, J. K. Thompson, and V. Vuletic , Interfacing Collective Atomic Excitations and Single Photons, Phys. Rev. Lett. 98, 183601 (1-4) (2007).
14. G.B. Jo, J.H. Choi, C.A. Christensen, Y.R. Lee, T.A. Pasquini, W. Ketterle, and D.E. Pritchard, Matter-Wave Interferometry with Phase Fluctuating Bose-Einstein Condensates, Phys. Rev. Lett. 99, 240406 (2007).
15. Wu S, Su E, Prentiss M, Demonstration of an area-enclosing guided-atom interferometer for rotation sensing , Phys. Rev. Lett. 99, 173201 (2007).

(b) Papers published in non-peer-reviewed journals

NONE

(c) Presentations
i. Presentations at meetings, but not published in Conference Proceedings
About 50 presentations a year

ii. Non-Peer-Reviewed Conference Proceeding publications (other than abstracts)

Wolfgang Ketterle:
New Frontiers with Ultracold Gases.
in: Atomic Physics 19, Proceedings of the XIX International Conference on Atomic Physics (ICAP) 2004, eds. L.G. Marcassa, K. Helmerson, V.S. Bagnato (American Institute of Physics, 2005) pp. 25-29.
iii. Peer-Reviewed Conference Proceeding publications (other than abstracts)

NONE

(d) Manuscripts

NONE

(e) Books

NONE

(f) Honor and Awards

W. Ketterle Killian Award, MIT, 2004
W. Ketterle German Academy of Natural Scientists Leopoldina, 2005
W. Ketterle Honorary Degree of Doctor of Science from Gustavus Adolphus College, 2005
Yong-Il Shin Deutsch Award for Excellence in Experimental Physics at MIT, 2005
W. Ketterle Fellow of the Optical Society of America, 2006
Yong-Il Shin Finalist in the competition for the 2006 APS award for Outstanding Doctoral Thesis Research in Atomic, Molecular, or Optical Physics, 2006
W. Ketterle Honorary Ph.D. Degree from the University of Connecticut, 2007
Huanqian Loh, Apker undergraduate thesis award of the American Physical Society

(g) Title of Patents Disclosed during the reporting period

Provisional patent for moving waveguide interferometer.

(h) Patents Awarded during the reporting period

NONE

(2) Student/Supported Personnel Metrics for this Reporting Period (name, % supported, %Full Time Equivalent (FTE) support provided by this agreement, and total for each category):

(a) Graduate Students
Ketterle group:
Yong-Il Shin
Tom Pasquini
Gyu-Boong Jo
Ye-ryoung Lee
Partially support, estimated FTE 1.0
Prentiss Group:
Pierre Streihl
Jonathan Gillen
Saijun Wu
Partially supported, estimated FTE 2
Vuletic Group:
Yu-ju Lin
Igor Teper
Haruka Tanji
Partially support, estimated FTE 1.0

(b) Post Doctorates
Ketterle group:
Michele Saba
Jae Hoon Choi

Partially supported, estimated FTE 0.7
Prentiss Group:
Pablo Londero
Partially supported, estimated FTE 0.5
Vuletic group
none

(c) Faculty

Ketterle, Wolfgang 30 %
Prentiss, Mara 30 %
Vuletic, Vladan. 30 %
Pritchard, David

(d) Undergraduate Students
Ketterle group:
Christian Sanner
Sebastian Will
Tony Kim
Prentiss Group:
Daniel Okobi
Edward Su
Alex Sloan
Vuletic Group:
Huanqian Loh
Brendan Shields
David Brown

(e) Graduating Undergraduate Metrics (funded by this agreement and graduating during this reporting period)
i. Number who graduated during this period
5 Edward Su, Alex Sloan, Huanqian Loh, Brendan Shields, David Brown

ii. Number who graduated during this period with a degree in science, mathematics, engineering, or technology fields
5

iii. Number who graduated during this period and will continue to pursue a graduate or Ph.D. degree in science, mathematics, engineering, or technology fields
4 Edward Su (MIT, PhD Physics), Huanqian Loh (U Colorado Boulder, PhD Physics), Brendan Shields (Harvard, PhD Physics), David Brown (Caltech, PhD Physics).

iv. Number who achieved a 3.5 GPA to 4.0 (4.0 max scale)
4

v. Number funded by a DoD funded Center of Excellence grant for Education, Research and Engineering
0

vi. Number who intend to work for the Department of Defense
0

vii. Number who will receive scholarships or fellowships for further studies in science, mathematics, engineering or technology fields
2

(f) Masters Degrees Awarded (Name of each, Total #)

Christian Sanner, Diploma thesis, University of Heidelberg, Germany, 2004
Sebastian Will, Diploma thesis, University of Mainz, Germany, 2006

(g) Ph.D.s Awarded (Name of each, Total #)

Yong-Il Shin, 2005
Tom Pasquini, 2007
Mukund Vengalattore 2005
Pierre Striehl 2007
Saijun Wu 2007
Igor Teper 2006
Yu-ju Lin 2007
(h) Other Research staff (Name of each, FTE % Supported for each, Total % Supported)
Faculty
Alex Sloan just after his undergraduate degree award.

(3) "Technology transfer" (any specific interactions or developments which would constitute technology transfer of the research results). Examples include patents, initiation of a start-up company based on research results, interactions with industry/Army R&D Laboratories or transfer of information which might impact the development of products.

Scientific progress and accomplishments

On the following pages, we highlight important projects done by the groups of W. Ketterle, M. Prentiss, and V. Vuletic within the gBECi program.

Ketterle group

1. Continuous measurement of the relative phase of two Bose-Einstein condensates using light scattering

We have demonstrated an experimental technique based on stimulated light scattering to continuously sample the relative phase of two spatially separated Bose-Einstein condensates of atoms [1]. This is the first time that the phase of a condensate could be determined in a non-destructive way. The phase measurement process created a relative phase between two condensates with no initial phase relation, read out the phase, and monitored the phase evolution.

By monitoring the phase of two condensates at two separated times, interferometry between two trapped Bose-Einstein condensates without need for splitting or recombining.

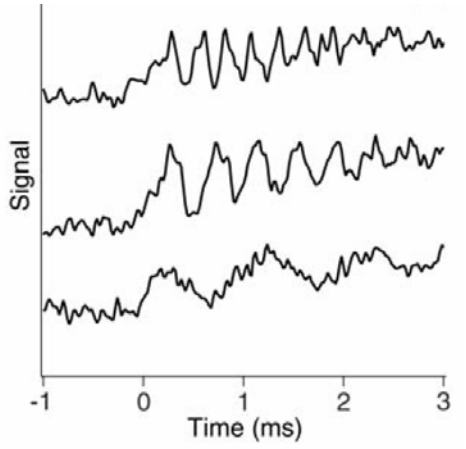

Continuous optical read-out of the relative phase of two condensates. The traces show that the intensity of the light scattered from the condensates oscillates in time. Bragg scattering starts at t =0 when the second beam is turned on. The relative depth of the two wells was different for the three traces, generating a difference in the beat frequency between the two condensates.

2. Optical Weak Link between Two Spatially Separate Bose-Einstein Condensates

The concept of Josephson coupling can be extended to include two spatially separate quantum systems by using intermediate coupling systems. The phase of the coupling may be actively controlled by adjusting the coupling states of the intermediate systems. We have experimentally demonstrate phase-sensitive optical coupling of two spatially separate Bose- Einstein condensates using Bragg scattering [2]. We have studied two

condensates in an optical double-well potential, irradiated by two pairs of Bragg beams which couple out beams of atoms propagating to the left or the right, respectively, and these unconfined propagating atoms constitute the intermediate coupling system in our scheme. Depending on the relative phases of the two condensates and the coupling states, we observe only one outcoupled beam propagating to one or the other side, or two identical beams propagating in opposite directions (see figure). This demonstrates phase control of currents and establishes a new scheme to realize Josephson effects with two non-overlapping condensates.

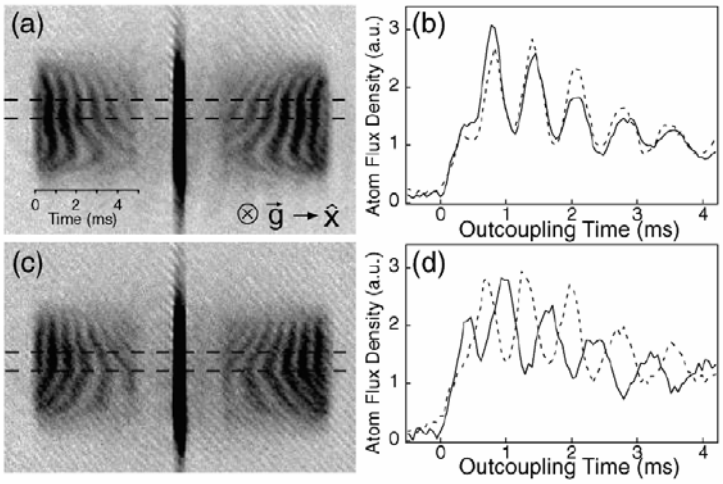

Symmetric and antisymmetric correlation between outcoupled atom patterns. Two pairs of Bragg beams outcoupled atoms in either +x or -x direction. Absorption images were taken after 5 ms outcoupling and 2 ms additional ballistic expansion. The left outcoupled atom patterns were compared with the corresponding right patterns. Depending on the frequency of the Bragg beams, we observed symmetric correlation between the two patterns (top) or antisymmetric correlations (bottom). The field of view is 0. 9 mm x 0.6 mm.

3. Interference of Bose-Einstein condensates split with an atom chip.

A major step towards compact matter wave sensors is an atom interferometer on an atom chip. We have used an atom chip to split a single Bose-Einstein condensate of sodium atoms into two spatially separated condensates [3]. Dynamical splitting was achieved by deforming the trap along the tightly confining direction into a purely magnetic double-well potential. We observed the matter wave interference pattern formed upon releasing the condensates from the microtraps. The intrinsic features of the quartic potential at the merge point, such as zero trap frequency and extremely high field-sensitivity, caused random variations of the relative phase between the two split condensates. Moreover, the perturbation from the abrupt change of the trapping potential during the splitting was observed to induce vortices.

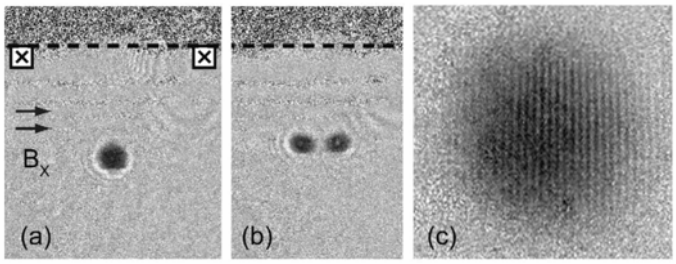

Splitting of condensates. (left) Condensates were initially loaded and prepared in the bottom well and (middle) split into two parts by increasing the external magnetic field. For clarity, two condensates were split by 80 μm. The dashed line indicates the chip surface position. (right) Two condensates were released from the magnetic double-well potential and the matter wave interference pattern of two condensates formed after time-of- flight.

4. The Role of Interactions in Quantum Reflection of Bose-Einstein Condensates

Quantum reflection is the phenomena by which an atom is accelerated so abruptly by the Casimir-Polder potential that it reflects from the potential rather than being drawn into the surface. The usual model of quantum reflection treats the atom-surface interaction as a single atom in a potential. However, in a recent study of quantum reflection of Bose-Einstein condensates (BECs), the reflection probability was limited to ~15% at low velocity [4]. A theoretical paper simulating quantum reflection of Bose-Einstein condensates could not explain the low reflectivity [5].

In this work, we have studied how inter-atomic interactions affect quantum reflection of Bose-Einstein condensates [6]. A silicon surface with a square array of pillars resulted in higher reflection probability than was previously observed with a solid silicon surface. For incident velocities greater than 2.5 mm/s, our observations agreed with single-particle theory. At velocities below 2.5 mm/s, the measured reflection probability saturated near 60% rather than increasing towards unity as predicted. We have extended the theory of quantum reflection to account for the mean-field interactions of a condensate which suppress quantum reflection at low velocity. Our model predicts improvements for longer healing lengths and how the corresponding reduction in condensate density sets a limit for the incident flux of atoms.

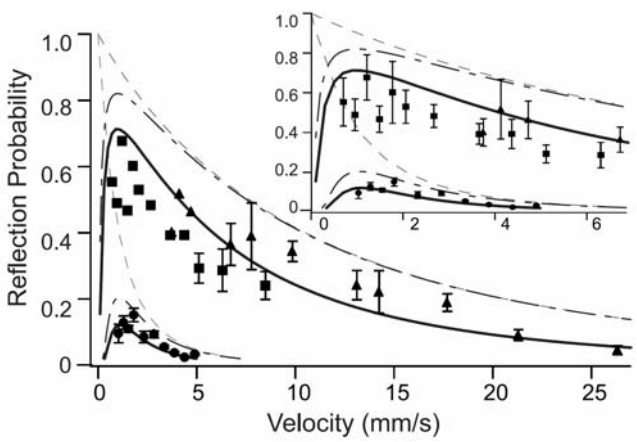

Reflection probability vs. incident velocity. Data are shown for a pillared (square) and solid (circle) Si surface. Single atom models give a monotonic rise to unity reflection. Our model which includes interactions (solid line) shows saturation of reflection at low velocity in qualitative agreement with our observations.

5. Long Phase Coherence Time and Number Squeezing of two Bose-Einstein Condensates on an Atom Chip

Precision measurements in atomic physics are usually done at low atomic densities to avoid collisional shifts and dephasing. This applies to both atomic clocks and atom interferometers. At high density, the atomic interaction energy results in so-called clock shifts and leads to phase diffusion in Bose-Einstein condensates. Operating an atom interferometer at low density severely limits the flux and therefore the achievable signal-to-noise ratio.

Here we show that we can operate a BEC interferometer at high density, with mean field energies exceeding h 5 kHz [7]. Using an radio frequency (RF) induced beam splitter we demonstrate that condensates can be split reproducibly, so that even after 200 ms, or more than one thousand cycles of the mean field evolution, the two condensates still have a controlled phase. The observed coherence time of 200 ms is ten times longer than the phase diffusion time for a coherent state, i.e., a state with perfectly defined relative phase at the time of splitting. Therefore, repulsive interactions during the beam splitting process have created a non-classical squeezed state with relative number fluctuations ten times smaller than for a Poissonian distribution

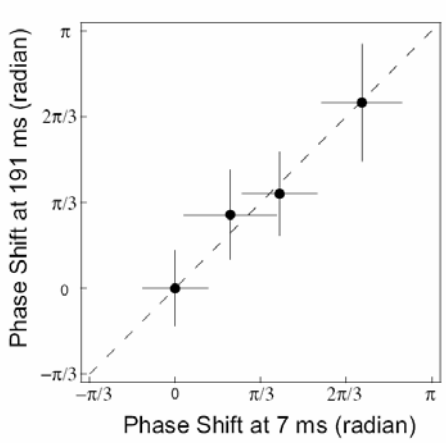

Long phase coherence of two separated condensates. Various phase shifts were applied on the condensates 2 ms after splitting by pulsing on an additional magnetic field. The shifts of the relative phase were measured at 7 ms and 191 ms, showing strong correlation. The dotted line denotes the ideal case of perfect phase coherence.

6. Guiding atoms with a hollow core photonic crystal fiber

In contrast to ordinary fibers, hollow core photonic crystal fibers guide light through vacuum. Red-detuned light in such a fiber can therefore act as a guide for ultracold atoms. We have done preliminary experiments where we loaded atoms into such a device. A sodium Bose-Einstein condensates was transported close to the fiber tip with optical tweezers, and was pulled into the fiber when the light through the fiber was ramped up, while the intensity of the tweezers beam was ramped down. Since the detection of atoms inside the fiber by direct imaging turned out to be infeasible, we retrieved some of the atoms by ramping up the light in the tweezers. Up to 5 % atoms re-appeared after having spent 30 ms in the hollow core fiber [8].

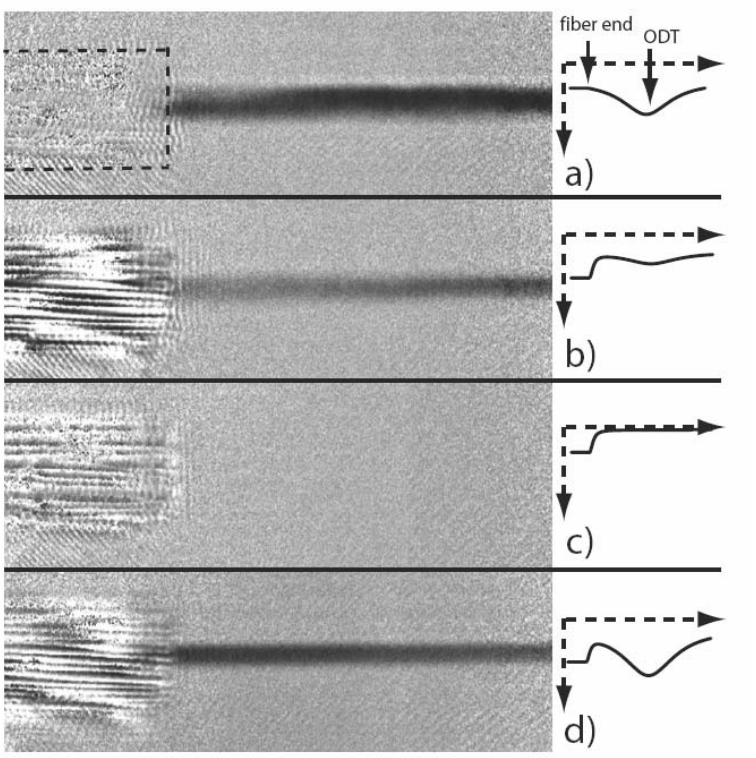

Images of atoms in the optical dipole trap (ODT) during the experiment. Also shown are sketches of the corresponding combined potential of the Hollow Core Fiber Trap (HCT) and ODT. (a) Atoms are held in the ODT near the fiber, with no light coupled into the fiber. The dashed line indicates the position of the 100 μm thick fiber. (b) Light is coupled to the fiber, and as the ODT intensity is ramped down, atoms are depleted from the ODT until (c) no atoms remain outside the fiber when the ODT power reaches zero. (d) After ramping the ODT back up, atoms that were trapped in the HCT return to the ODT.

7. Phase Sensitive Recombination of Two Bose-Einstein Condensates on an Atom Chip

Most experiments in atom interferometry use freely propagating atom clouds. Alternative geometries are confined-atom interferometers where atoms are guided or confined in trapping potentials, often realized by using atom chips. Many discussions of confined-atom interferometers proposed a readout by merging the two separated atomic clouds, but it was also shown that the recombination process is very sensitive to atomic interactions which can lead to exponential growth of unstable modes.

The present work demonstrates that interactions between atoms and collective excitations are not necessarily deleterious to direct recombination of separated trapped condensates that have acquired a relative phase in atom interferometry. We show that in-trap recombination leads indeed to heating of the atomic cloud. However, this heating is phase dependent and can be used as a robust and sensitive readout of the atom interferometer. The resulting oscillations of the condensate atom number are dramatic (typically ~25% contrast), occur over a wide range of recombination rates, and permit high signal to noise ratios since they simply require a measurement of the total number of condensate atoms in the trap [9].

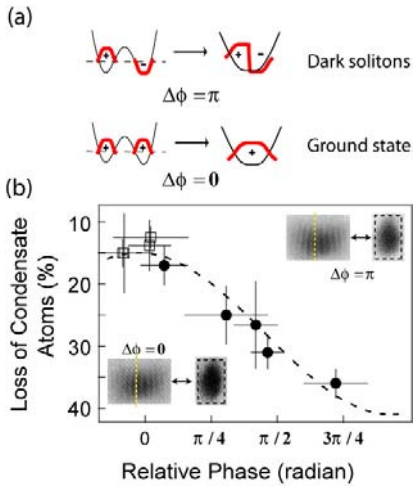

Concept and results on phase-sensitive recombination of two condensates. (a) The merged matter-wave functions are shown for the case of a sudden merger of interacting condensates leading to soliton formation for a relative phase of Pi. (b) The relative phase of two split condensates was monitored for various hold time after splitting by suddenly releasing the two condensates and observing interference The heating during recombination (observed through the loss of condensate atoms) was correlated with the relative phase and can be used as in situ read out the atom interferometer.

8. Matter-Wave Interferometry with Phase Fluctuating Bose-Einstein Condensates

A non-interacting zero-temperature Bose-Einstein condensate is the matter-wave analogue to the optical laser, and therefore the ideal atom source for matter-wave interferometry. However, at finite temperature elongated condensates (e.g. in wave guides) suffer from phase fluctuations.

We observed directly axial phase fluctuations and characterized their effect on the coherence time of the atom interferometer. We demonstrated that atom interferometry can be performed in the presence of phase fluctuations [10].

We found some degradation of the fringe contrast due to phase fluctuations. However, it appears that for our experimental conditions, this degradation is not due to the quantum limit of phase fluctuations, but is rather caused by asymmetries in the double-well potential leading to relative motion of the divided condensates.

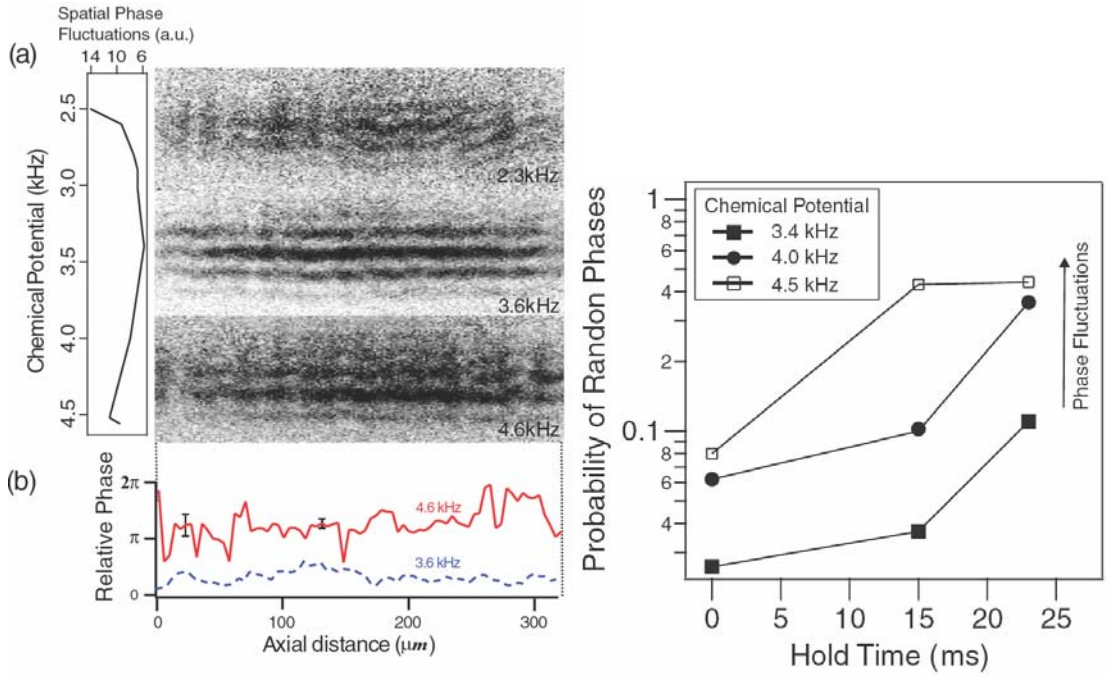

Effect of longitudinal phase fluctuations on the performance of the matter-wave interferometry.
(Left) Effect of spatial phase fluctuation on the waviness of interference fringes. Interference fringes obtained right after splitting a condensate in (a). For large spatial phase fluctuation (e.g., 4.6 kHz), the fringe pattern shows more significant wiggles than for smaller phase fluctuations (e.g.,3.6 kHz). From the fringes for 3.6 kHz (dashed line) and 4.6 kHz (solid line) chemical potentials, relative phases are obtained along the axial direction in (b)
(Right) Effect of longitudinal phase fluctuations on the coherence time between the split condensates. The probability for a random phase for ten measurements of the relative phase is shown for three different amounts of the longitudinal phase fluctuations.

Prentiss group

1. Continuous non-destructive measurement of interferometer phase using light scattering

The Bragg scattering due to atom interference produces a backscattered optical beam whose phase depends on the spatial phase of the atom interferometry signal. Heterodyne detection that demodulates the beat produced by combining the backscattered Bragg light with frequency shifted light produces a continuous non-destructive measurement of the phase of the atom interference pattern. [11]

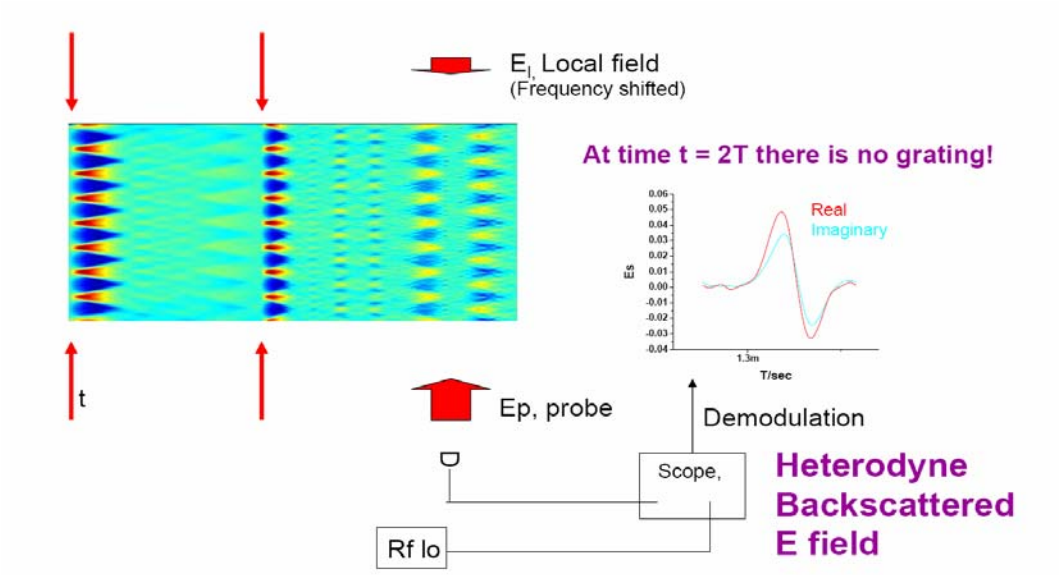

Caption: Left is the schematic of a three pulse atom interferometer where the atomic beam progates from left to write and the color represents the atom density as a function of position. Red represents high density, dark blue represents low density and green represents uniform density. The narrow red arrows show the locations of the otpical standing wave pulses, and the broad red arrows show the location of the probe field whose backscattering by the atomic density distribution was detected by measuring the heterodyne signal due to the beating between the probe and the frequence shifted local field. The inset shows the actual measured in phase and quadrature components of the demodulated field, which measures the spatial phase of the atomic density distribution in the atom interferometer.

2. Demonstration of a Compact High Flux Atom Source

Zeeman slowers produce very high flux slow atom sources, but they are large and cumbersome making them unsuitable for most rotation sensor applications. We used a two dimensional MOT created by poled ferromagnetic foils to create a compact, slow, high flux Rb87 atom source suitable for the continuous loading of magnetic waveguides. The experimentally measured flux as a function of the most probable beam velocity is shown in the figure below, where the length of the source 3.4×4.4×7 cm and the beam divergence was 40 mRad.[12]

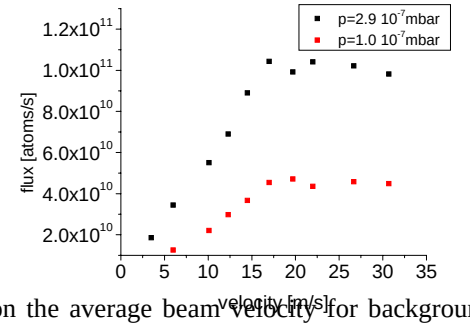

Caption: Flux dependence on the average beam velocity for background pressures of $1 \cdot 10^{-7}$ mbar and $2.9 \cdot 10^{-7}$ mbar

3. Demonstration of an Area Enclosing Two-Dimensional Unguided Atom Interferometer

Previous area enclosing interferometers have used a beamsplitter to create velocity in one direction ,while using the center of mass motion of the atom sample to provide motion along a second axis. Thus, the velocity in one direction was well defined by the bemasplitter, but the motion in the other direction was not. In this experiment, we used optical beamsplitters to created motion in two dimensions, resulting in well defined velocities in both directions. Various light pulse schemes were considered, some of wich are demonstrated in the schematic below. [12]

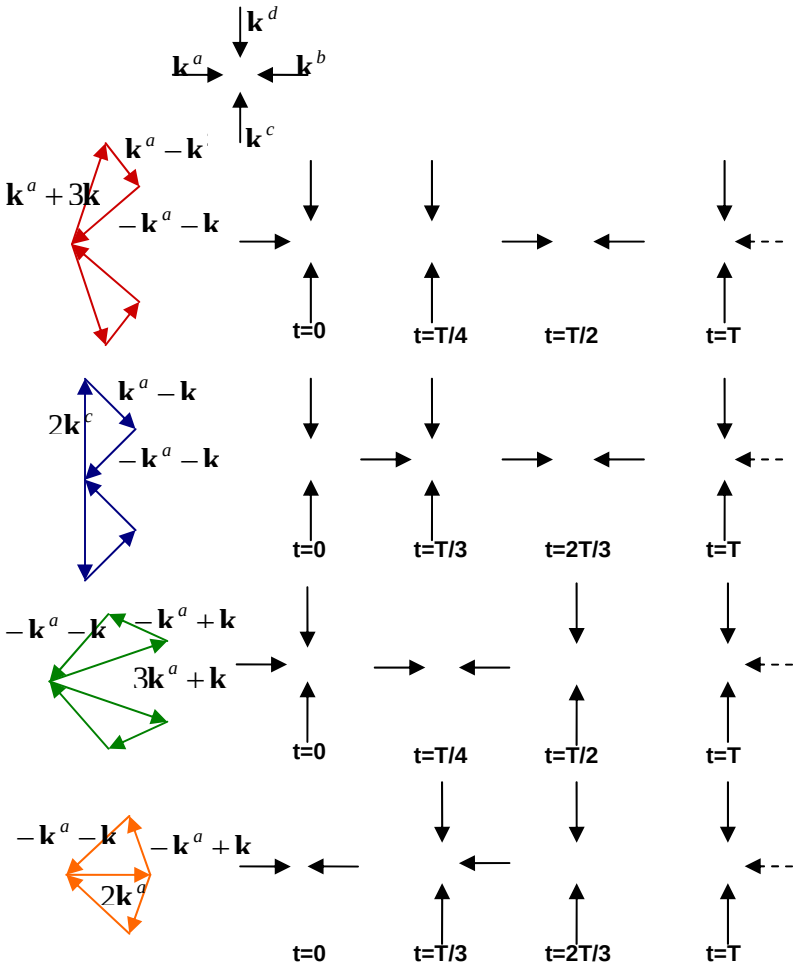

Caption: Different loops in momentum space (left) and the corresponding sequences of standing wave pulses (right). The last pulse in every sequence represents the readout pulse, the dotted arrow signifies weak light that serves as a local oscillator for analyzing the backscattered signal using a heterodyning technique.

The temporal pulse sequence and phase readouts for one such loop set are shown below.

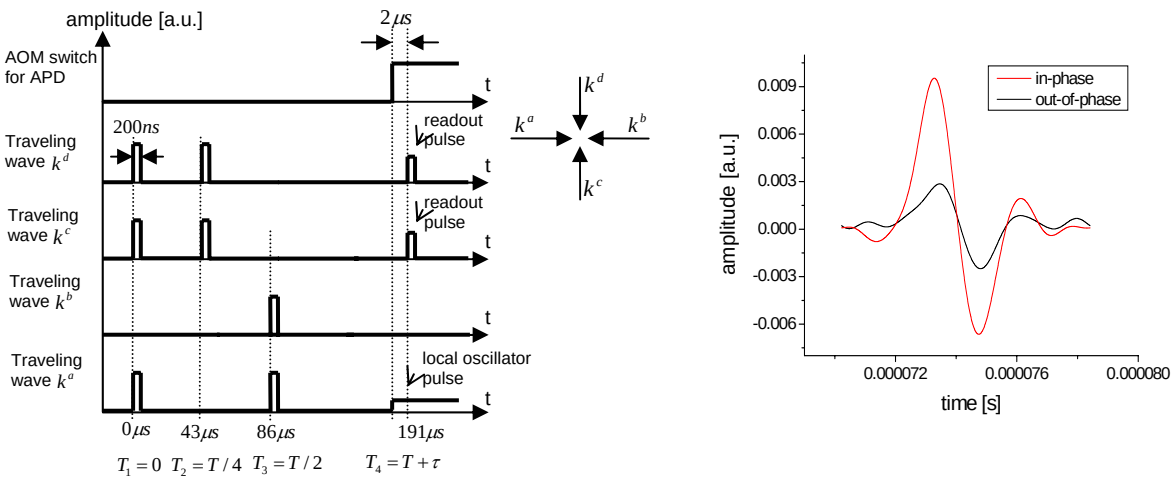

Caption: At left, time-sequence of the standing wave pulses for the 2-D Talbot-Lau interferometer (loop 1). At right digitally demodulated backscattering signal at T=185 μs . The modulation of the signal was achieved by mixing the backscattered light with light from the second traveling wave that was modulated at 6Mhz.

4. Demonstration of a Reciprocal Path Area Enclosing Guided Atom Interferometer using a Moving Waveguide

We demonstrated that the coherence between atomic wavepackets split by optical beamsplitters is preserved even when the wavepackets are confined in magnetic waveguides. We showed that this result holds for both condensate and non-condensate atoms as long as the waveguide is straight. Sadly, such atom interferometers enclose no area, so they cannot be used as gyroscopes; however, if the magnetic guide is translated along the direction perpendicular to the guiding direction, then the resulting interferometer will enclose area. If the beamsplitter pulses are applied at times T/4 and 3 T/4 and the direction of the waveguide motion is reversed at time T/2, then the resulting interferometer paths will enclose area and be reciprocal. Thus, the phase of the interferometer will be sensitive to rotation, but insensitive to any time independent acceleration. A schematic of this system is shown below. [13]

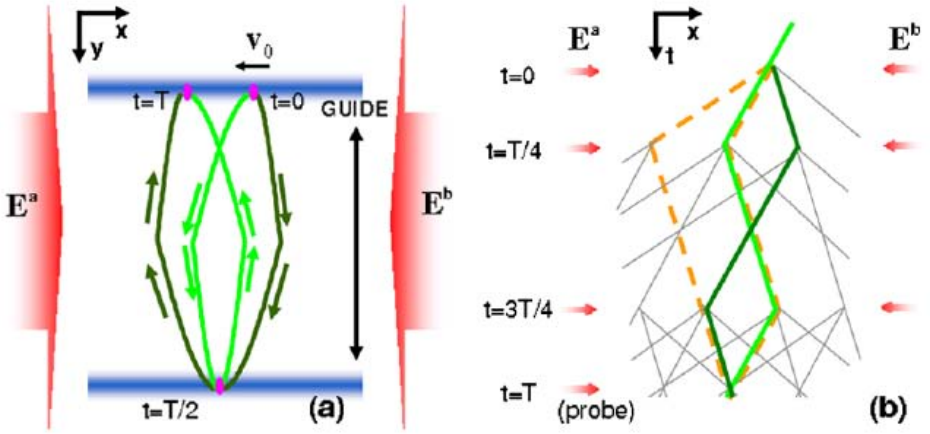

Caption: (a) Schematic of a moving-guide interferometer. The two horizontal blue bars represent the position of the moving guide at times *t* _ 0, *T* (top) and *t* _ *T*=2 (bottom),with the center-of-mass position of a guided atomic wave packet at the three times marked. The optical fields E*a* and E*b* are pulsed [see (b)]. The atom follows the thick solid curve to interfere at time *t* _ *T*. (b) The *x*-*t* recoil diagram for the fourpulse scheme. At time *t* _ *T* the atomic fringe is probed via a Bragg-scattering from E*a* to E*b*. The figure 8 interfering loop marked with thick solid lines corresponds to that in (a). The orange dotted lines correspond to the trapezoid loop, which is not reciprocal.

The phase readout for the reciprocal figure 8 loop and the trapezoid loop are shown below as a function of time for the case where the waveguide is not moving, so the loop encloses no area. The waveguide had a slight tilt with respect to gravity, so the trapezoidal loop has a gravitationally induced phase shift that is quadratic as a function of time. In contrast, the phase shift for the reciprocal loop is independent of time. The reciprocity of the figure 8 loop results in an improved coherence time, so at long times the only interferometer signal is due to the reciprocal loop, whereas at short times the contribution to the non-reciprocal trapezoidal loop dominates.

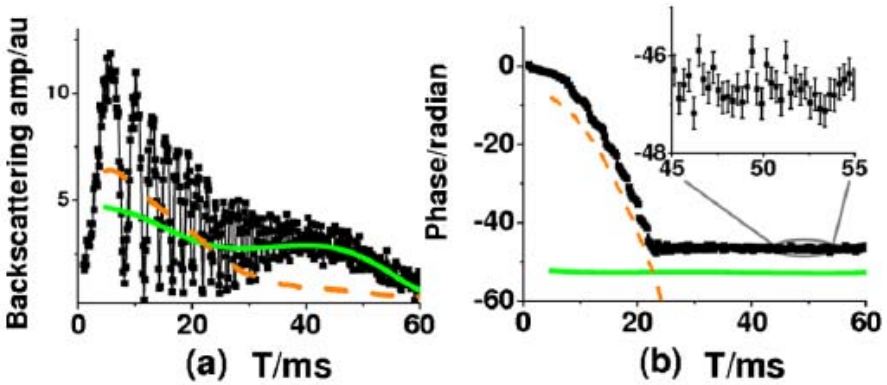

Caption Four-pulse interferometry readout in a stationary guide. The four-pulse data (black) is decomposed into the solid and the dashed curves that correspond to the contributions from the figure 8 and trapezoid loops in Fig. 1, respectively. (a) Interferometry amplitude (b) Interferometry phase with an inset plot around 50 ms. The phases in (b) have been unwrapped. The error bars give the phase noise due to mirror vibrations.

The figure below demonstrates the phase coherence of the interferometer for the case where the waveguide is moving, so that the interferometer does enclose area. The actual ferromagnetic structure that produced the magnetic waveguide remained stationary,

but the magnetic zero that defines the location of the waveguide was translated by varying the the current used to pole the ferromagnetic material as a function of time.

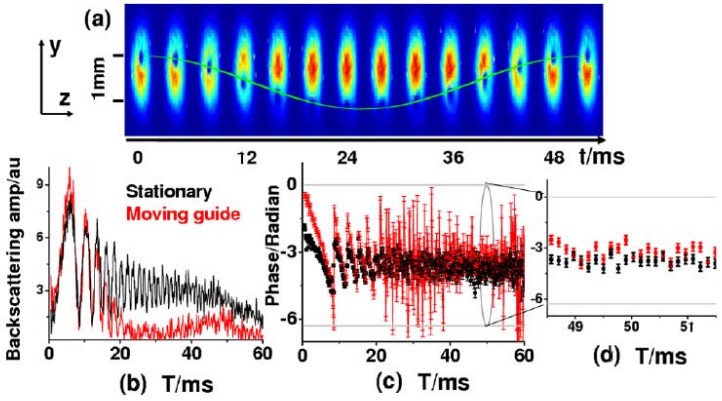

Caption: Top: Absorption images of the guided atomic sample following the moving guide in 50 ms. The graphs are expanded along the **e***y* direction for clarity. A cosine curve is added as a guide for the readers' eyes. Bottom: Interferometer signals for the case of stationary (black) and moving (red/gray) guides. In (c), (d) the error bars indicate the standard phase deviation due to mirror vibrations. Notice the scale difference between Fig. 3(b) and (c) here.

5. Development of a Chip Based Moving Guide

Though the ferromagnetic structure used in the work decribed above is fairly compact ad provided a reasonable translation distance , a chip based version that used the time dependent current in an array of wires to produce the moving potential could provided larger areas in a more compact device. The figure below shows the calculated potentials as a function of time for a waveguide array, where the time dependent current in the wires in the array is adjusted to preserve the field gradient of the waveguide and to keep the separation between the waveguide and the chip constant as the waveguide is translated across the chip.[12]

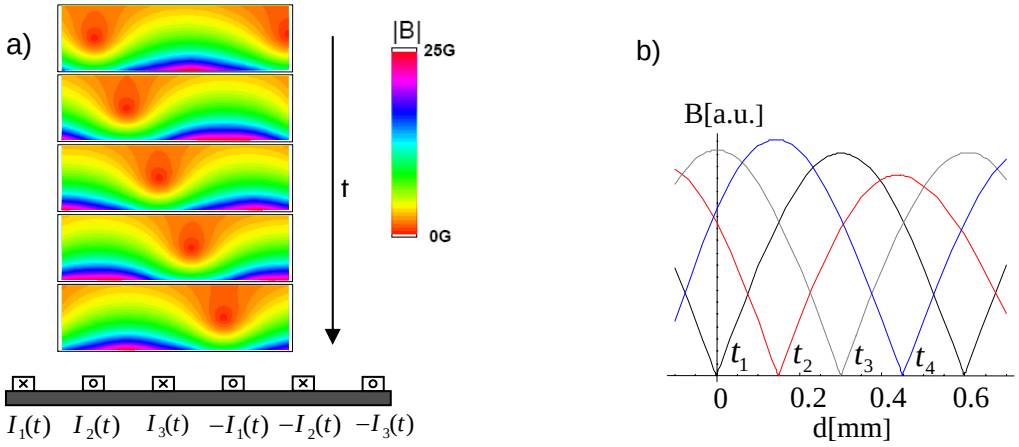

Caption: a) Contour plots of the total magnetic field as the guide moves smoothly across the chip (h=200 μm). Changes in the transverse gradient that occur during the movement (see figure 2) have been compensated for by multiplying the currents in all wires with the same time-dependant factor. b) Trap displacement in transverse direction at different times t_1 (black), t_2 (red), t_3 (gray) and t_4 (blue) for h=200

6 Demonstration Long Phase Coherence Time of Thermal Atoms Confined in a Magnetic Waveguide

In the moving waveguide experiments the enclose area was limited by the coherence time of the atoms in the guide; therefore, it is important to determine whether the decoherence is due to the wavepacket separation or just due to time. In the classic there pulse interferometer scheme, the separation and the time are coupled; however, the separation and time can be decoupled by using a four pulse interferometer. A schematic of the four pule interferometer is shown at the left below, and the resulting interferometer signal is shown at the right, where the for a wavepacket separation of 0.413 microns, the interferometer signal is visible for longer than one second. Thus, the phase coherence between the wavepackets is not disturbed by the confinement in the magnetic guide, it is only the separation between the wavepackets that results in decoherence because of spatial variations on the guiding

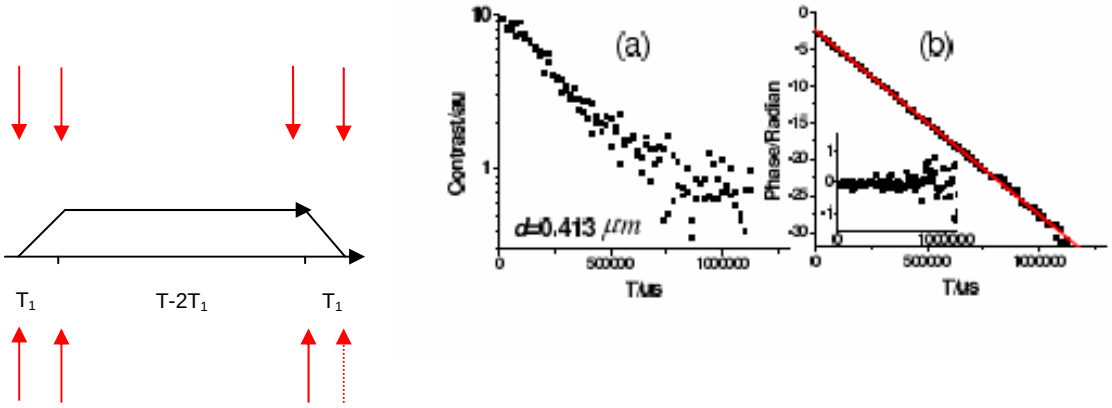

7 Demonstration that Quantum Freeze Reduces the Sensistivity of the Interferometer to Angular Misalignment Bewteen the WaveGuide and the Beamsplitter Pulses

If there is a misalignment between the beamsplitter direction and the guiding direction, then the application of the beamsplitter will result in the transfer of wavepackets between transverse waveguide modes resulting in decoherece. This problem can be solved by using a single mode waveguide; however, because the waveguide energies are quantized, there is an angle below which the beamsplitter pulses can no longer excite transverse modes. Thus, perfect coherence does not require perfect alignment, it only requires that the alignment be better than the threshold for the excitation of transverse modes. Notice that contrast decay as a function of angle is the same for all T>10 ms, showing that the decay is indeed frozen.[11]

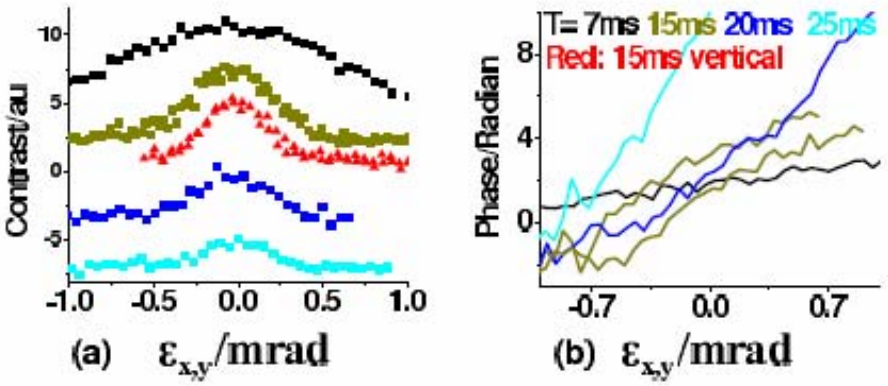

Caption: (a) Black, Brown, Blud, and Light blue plots of the contrast as a function of the intereferometer interrogation time T correspond to T=7 ms, 15 ms, 20, ms and 25 ms as the horizontal angle si scanned over a milliard across the optical waveguide/beamsplitter alignment. The red triangle plot give the T=15 ms angular tuning along the vertical axis with the horizontal axis optimized. The contrast curves are displaced along the y axis for clarity. B) phase shift $\phi(T)$ for the same set of data with the same color code.

Vuletic group

1. High-brightness, narrowband source of identical photon pairs

We have developed an atomic-ensemble source of photon pairs with spectral brightness near fundamental physical limitations and approximately three orders of magnitude greater than the best current devices based on nonlinear crystals. Unlike parametric down-converters, however, the atomic ensemble can additionally act as a quantum memory and store the second photon, allowing triggered (i.e., deterministic) generation of the second photon. Triggered delays of up to 20 μs have been demonstrated, and it is expected that optical lattices hold the potential to extend the lifetime of these quantum memories to seconds. Lastly, proposed applications in quantum information rely on joint measurements of single photons for which photon indistinguishability is crucial for high fidelity. We observe large degrees of indistinguishability (90%) in the time-resolved interference between the two generated photons.

The experimental setup consists of a laser-cooled ensemble of 10^4 Cs atoms in the TEM_{00} mode of a low-finesse (F=250), single-mode optical cavity (Fig. V1). Photon pairs are generated by a four-wave mixing process that relies on quantum interference in the emission from an entangled atomic ensemble to enhance the probability of scattering a second (read) photon into the cavity to near unity given the initial scattering of a (write) photon into the cavity (Fig. V1). Without collective enhancement, the maximum probability that the read photon would be scattered into the cavity was only 7.3×10^{-4}, and was nearly three orders of magnitude lower than the observed value of 0.57(9).

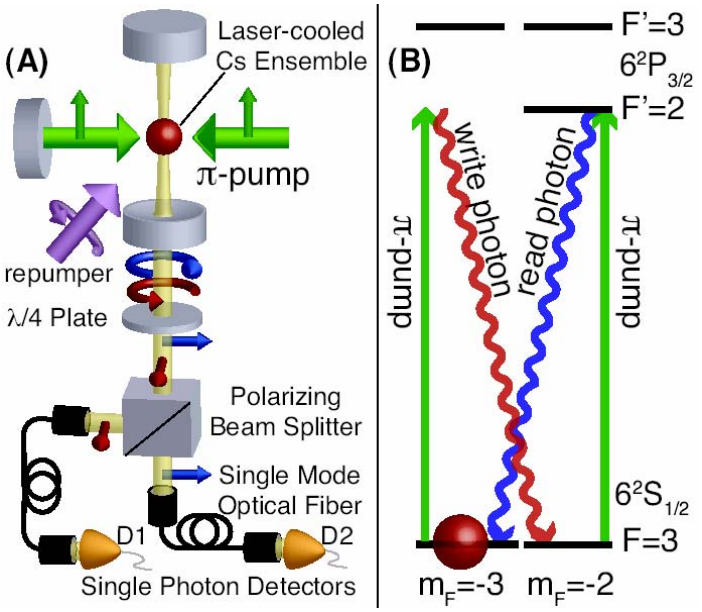

Fig. V1. (A) Experimental setup and (B) quantum states used for photon pair generation. The tuning of the π-pump laser is chosen so that the rate of write-photon scattering into the cavity is suppressed by a large detuning from resonance with any excited state, while the collectively stimulated generation of a read photon in the cavity proceeds rapidly via resonant coupling. This ensures that the time separation between subsequent pairs exceeds the time separation of the write and read photons within a pair – leading to large cross correlations between the photon polarizations. The pump and emitted-photon polarizations are denoted by the smaller arrows. The π-pump in combination with a repumper (tuned to the ground F = 4 to excited F' = 4 transition) optically pump approximately 95% of the atomic population into $|F = 3, m_F = -3\rangle$.

To first verify that the light emitted in one polarization is correlated in time with the light in the other polarization, we measure the second-order correlation function $g_{wr}(\tau)$ between the write and the read light, averaged over a bin of length T = 10ns (Fig. V1). This is simply the measured coincidence count rate between the detectors D1 and D2 normalized by the rate one would expect for two completely uncorrelated beams of the same average intensities. τ specifies a time offset between the write and read windows. The time-resolved cross correlation has peak coincidence rates 100(10) times higher than for uncorrelated beams.

To further quantify the performance of the photon-pair source, we measure the conditional probability that a read photon is emitted by the sample given that a write photon has been observed. A lower bound on this read recovery efficiency R is obtained from the measured detection losses q_r, combined with the measured probability of detecting a read photon given the detection of a write photon R_{cond}^{det}. The physical recovery efficiency for a cavity of the same linewidth, but with losses completely

dominated by transmission of one of the two mirrors, is $R_{cond} = R_{cond}^{det} / q_r = 0.57(9)$. Given the low finesse F = 250 of the present cavity, this ideal regime could be easily achieved with current technologies.

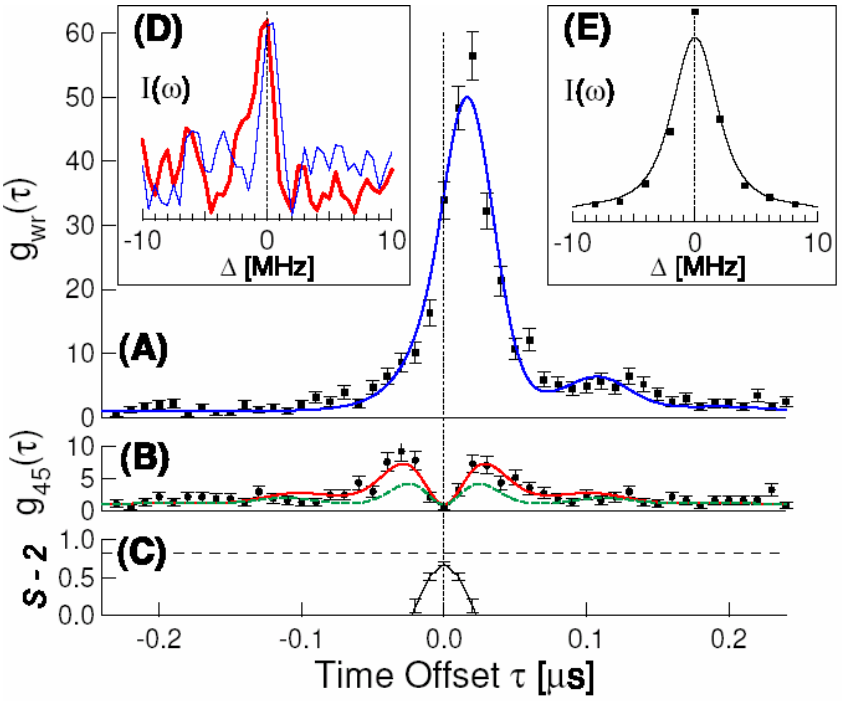

Fig. V2. Measures of identicalness and photon frequency bandwidths. (A) The time-resolved cross correlation function $g_{wr}(\tau)$ and (B) the same function $g_{45}(\tau)$ measured in a polarization basis rotated by 45°. In the 45° basis, coincidence events are suppressed by two-photon interference resulting from the near-indistinguishability of the photons. Assuming the photons have identical frequencies, the quantity $g_{45}(\tau)$ can be predicted directly from $g_{wr}(\tau)$ (green dashed curve in (B)). The prediction is more accurate if a photon frequency difference $\Delta\omega/2\pi$ = 2.5 MHz is assumed (red curve in (B)). (C) The predicted violation of a Bell's inequality $S-2 < 0$ if the photon pairs were used to produce polarization-entangled photons. The dashed line is the maximum possible violation. (D) The frequency bandwidths of the write (red) and read (blue) photons are determined to be 1.1(2) MHz from the displayed heterodyne beat notes. For comparison, (E) shows the square of the Fourier transform of $(g_{wr}(\tau) - 1)^{1/2}$ taken at different parameters, indicating that the photon bandwidths are nearly transform limited.

2. Single-atom detection on a microchip

For an interferometer to achieve its full performance, the atomic-state readout should be performed at the atomic shot-noise limit. We have implemented single-atom detection on a microchip using both fluorescence and absorption methods, and compared their performance.

For the fluorescence measurement, we illuminate the atoms with a retroreflected pump beam resonant with the D_2 line, and measure the number of photons scattered into the resonator in 250 μs. By analyzing histograms of the number of detected photons, we can extract independently the average number of atoms prepared in the trap, and the average number $\langle p \rangle$ of photon counts per atom. We find that we register $\langle p \rangle = 1.4(3)$ counts per atom, at a background count of $\langle b \rangle = 0.07$. This means that, if we set our detection threshold to ≥1 count, our single-atom detection is characterized by an atom quantum efficiency of 75% and a false detection rate of 7%, at a maximum single-atom count rate of 4 kHz.

While the fluorescence measurement makes a good single-atom detector, we expect an absorption measurement to provide better atom number resolution for atom numbers $a>1$. For absorption detection, we couple the probe laser beam into the cavity TEM_{00} mode and monitor the resonant transmission through the cavity in the presence of atoms. Similarly to fluorescence detection, we compile histograms collected in 1 ms for different atom preparation parameters and fit them, assuming Poisson statistics for both the atoms and the photons per atom, to determine the mean absorption per atom $\langle s \rangle$. We find $\langle s \rangle = 3.3(3)\%$, in good agreement with the expected absorption per atom, $\langle s \rangle = 3.2(7)\%$.

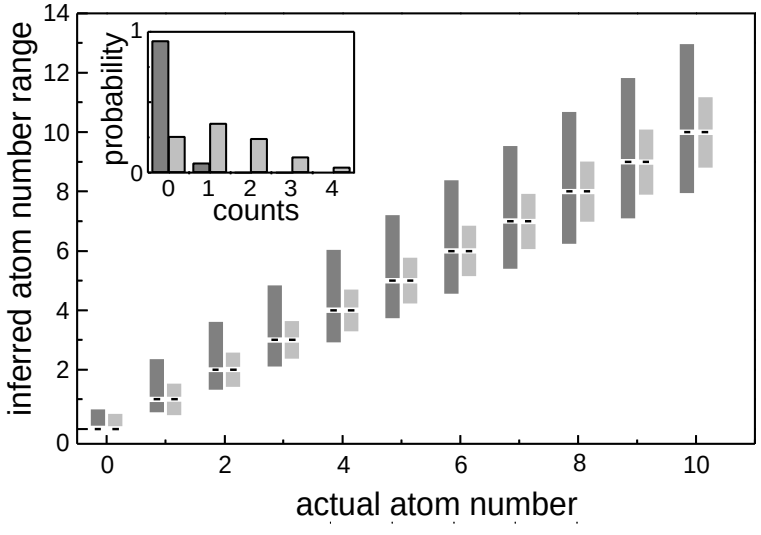

Fig. V3. Single-shot atom number measurement 1-σ confidence intervals for fluorescence (dark gray) and absorption (light gray). The inset shows computed normalized photon count distributions due to

background counts (dark gray) and to photons collected from one atom (light gray) for fluorescence single-atom detection.

Using the measured values for fluorescence and absorption, we can evaluate how well these two methods can determine the atom number in a single measurement. The expected atom number uncertainty Δa using fluorescence (absorption) detection due to both photon shot noise and the statistical uncertainty in the mean number of photons per atom $\langle p \rangle$ (uncertainty in the mean absorption per atom, $\langle s \rangle$), as well as the background photon counts (for fluorescence only), is plotted as a function of atom number in Fig. V3; the figure also includes a computed normalized histogram that characterizes the single-atom detection capability of our fluorescence measurement. For fluorescence, the atom number resolution is limited by the shot noise of the collected signal photons, which grows with atom number, while, for absorption, where the number of collected photons actually decreases with atom number, the resolution remains nearly flat, at around 1 atom.

3. Generation of states with reduced quantum uncertainty for an atomic clock

A two-level system can be formally described as a (pseudo-)spin s=1/2. In a typical precision experiment, the energy difference between the two levels is measured as a quantum mechanical phase accumulated in a given time. The result is read out as a population difference that can be formally viewed as the z-component S_z of the ensemble spin vector $\boldsymbol{S} = \sum \boldsymbol{s}_i$, where the sum is over the individual particles. The projection noise ΔS_z can be reduced by entanglement [14-17], by redistributing quantum noise from the S_z spin component to another spin component that is not directly affecting the experiment precision ("spin squeezing" [16-18]).

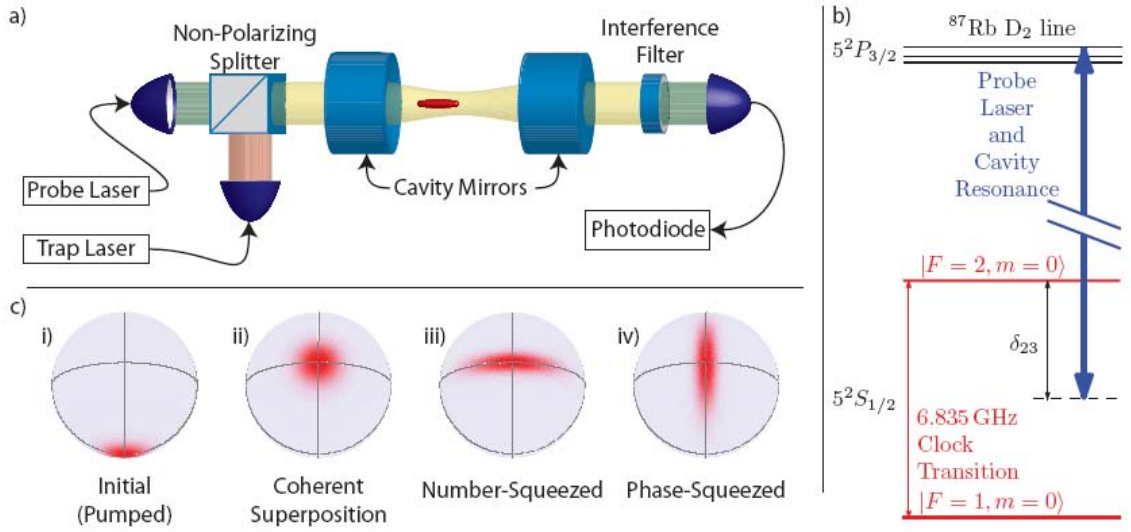

Figure V4. Measurement-induced pseudo-spin squeezing on an atomic clock transition. (a) Setup. A laser-cooled ensemble of ^{87}Rb atoms is loaded into a far-detuned optical dipole trap inside an optical resonator. The ensemble can be prepared in a superposition of hyperfine clock states $|1\rangle=|F=1,m_F=0\rangle$, $|2\rangle=|F=2,m_F=0\rangle$ by microwave pulses. A population difference N produces a resonator frequency shift that is measured with a probe laser. **(b) Atomic level structure.** The resonator is tuned such that atoms in the two clock states produce equal and opposite resonator frequency shifts via the state-dependent atomic index of refraction. **(c) Preparing a squeezed input state for an atomic clock.** A number-squeezed state (iii) can be generated from an unentangled state (coherent spin state, CSS) along x (ii) by measurement of N. It can then be rotated by a microwave pulse into a phase-squeezed state (iv), allowing a more precise determination of the phase acquired in the free evolution time of the atomic clock.

Spin squeezing requires an interaction between the particles [18] that can be achieved by collective coupling of the ensemble to a light field, provided the sample's optical depth (opacity if probed on resonance) is sufficiently large. Under appropriate conditions, the light-atom interaction entangles the ensemble spin $\boldsymbol{S}$ with the electromagnetic field, and a subsequent field measurement can then project the atomic ensemble into a spin-squeezed state. Such conditionally spin-squeezed input states can improve the sensitivity of a precision measurement device such as an atomic clock.

To prepare a spin-squeezed input state to an atomic clock, we adapt the proposal by Kuzmich, Bigelow, and Mandel [19] for a quantum non-demolition (QND) measurement of S_z with far off-resonant light. An ensemble of up to 10^5 laser-cooled ^{87}Rb atoms is optically trapped inside an optical resonator that serves to enhance the signal and optical depth (Fig. V5). One resonator mode is tuned such that the state-dependent atomic index of refraction produces a mode frequency shift that is proportional to the population difference $N = N_2 - N_1 = 2S_z$ between the hyperfine clock states $|1\rangle = |5S_{1/2},F=1,m_F=0\rangle$ and $|2\rangle = |5S_{1/2},F=2,m_F=0\rangle$. Then a QND measurement of S_z can be performed by

measuring the transmission of a weak probe beam through the ensemble-resonator system. A frequency stabilization system for probe laser and resonator ensures that the probe transmission noise is close to the photocurrent shot-noise limit.

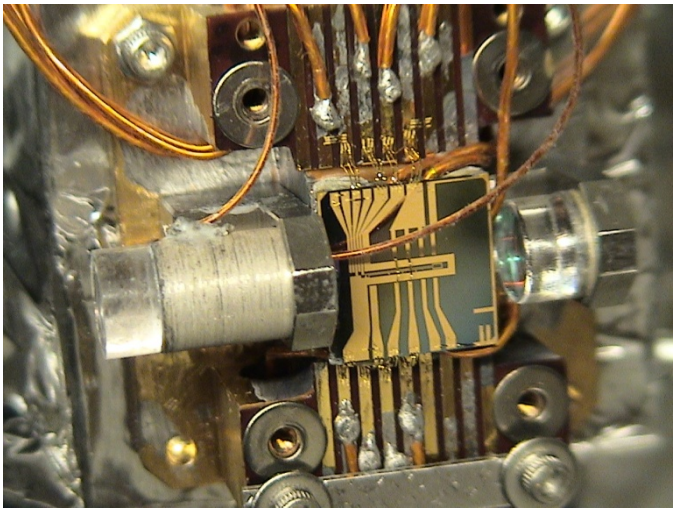

Figure V5. Microfabricated chip with mounted optical resonator. The resonator mode is aligned 200 μm above the surface of the microchip. The left mirror is mounted on a piezoceramic tube for tuning of the resonance frequency. The resonator finesse is $F = 8000$.

For an ensemble spin vector $\boldsymbol{S}$ oriented along the x axis, a state is spin squeezed [18] along the z-direction (or "number squeezed") if the uncertainty ΔS_z obeys $(\Delta S_z)^2 < |\langle S_x \rangle|/2$. For a maximally coherent system with $|\langle S_x \rangle| \approx S_0$, where $S_0 = N_0/2$ is the maximum possible spin of the ensemble containing N_0 particles, spin squeezing corresponds to a situation where the variance $(\Delta N)^2$ of the population difference $\Delta N = N_2 - N_1 = 2S_z$ between the two states $|1\rangle$, $|2\rangle$ is less than the projection noise limit, $(\Delta N)^2 < N_0$. However, since in real systems coherence (i.e. interference contrast) is often reduced, such that $|\langle S_x \rangle| < S_0$, spin-noise suppression below the projection noise limit $(\Delta S_z)^2 < |\langle S_x \rangle|/2$ is only a necessary but not a sufficient condition for spin squeezing. Thus to demonstrate spin squeezing one must measure both the spin noise ΔS_z, and the magnitude of the spin vector $|\boldsymbol{S}|$.

Fig. V6 shows the projection noise for an unentangled state of uncorrelated atoms (coherent spin state, CSS), and the quantum noise for a conditionally prepared entangled state with a random, but known value of S_z. For the former (red data points) the linear

dependence of $(\Delta S_z)^2$ on total atom number N_0 shows that we have prepared a state at the projection noise limit. For the latter, at low atom number the measurement noise exceeds the SQL due to photon shot noise and some technical noise (dash-dotted green line in Fig. V6), while at higher atom number $N_0 = 3\times10^4$ we achieve a 9 dB suppression of spin noise below the SQL.

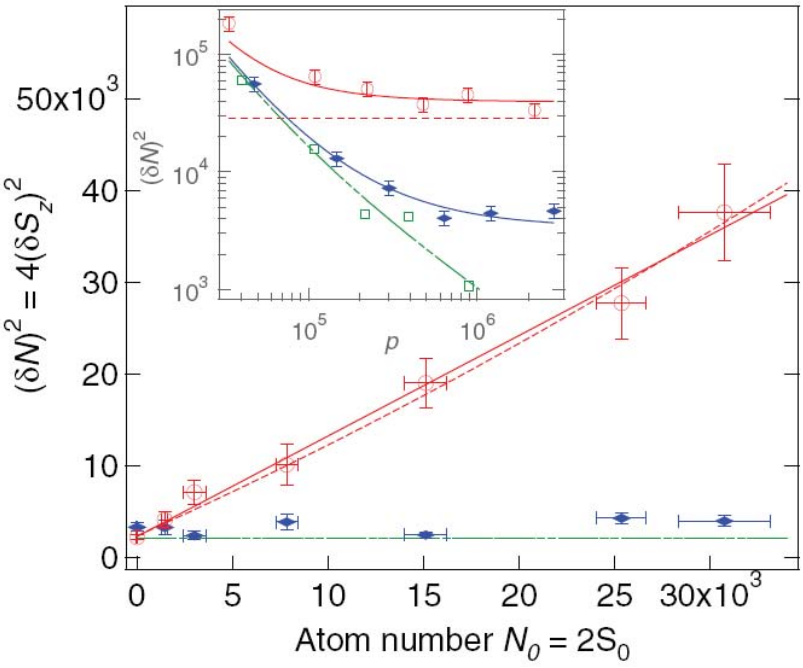

Figure V6 Projection noise limit and spin noise reduction. The measured spin noise for an uncorrelated state (CSS, open red circles) agrees with the theoretical prediction $(\Delta S_z)^2=S_0/2$, with negligible technical noise (solid and dashed red lines). Our measurement of S_z at photon number $p=5\times10^5$ has an uncertainty $(\delta S_z)^2$ (solid blue diamonds) substantially below the SQL. Inset: Dependence of spin measurement $(\delta S_z)^2=(\delta N)^2/4$ on probe photon number p for $N_0=3\times10^4$. With increasing photon number, the measurement uncertainty (solid blue diamonds) drops below the projection noise level (dashed red line). Also shown is the technical noise without atoms expressed as an equivalent spin noise (open green squares).

The reduction of ΔS_z below the SQL is accompanied by a substantial increase in ΔS_y. The shape of the uncertainty region can be verified by rotating the state prepared by the squeezing pulse by a variable angle about $\langle \boldsymbol{S} \rangle$ before performing the second S_z measurement. The variance $(\Delta S_\alpha)^2$ thus obtained is displayed in Fig. V7. The data are well described by a model that assumes the spin noise after the first measurement to constitute an ellipse with its short axis along z (solid blue line). The uncertainty area $A = \Delta S_z \, \Delta S_y$ is well above the Heisenberg limit $A_H = |\boldsymbol{S}| /2$ (dashed green line). The larger uncertainty is primarily due to the atomic-projection-noise-induced resonator shift, which

produces fluctuations in probe transmission well above the photon shot noise limit, resulting in substantial differential light shifts between the clock states. This effect, though not currently a limitation on our squeezing performance, can be reduced in future experiments by measuring on cavity resonance, or by using a feedback technique that keeps the transmitted photon number constant.

When we compare the observed squeezing to the reduction of clock signal $|\boldsymbol{S}|$, measured via the clock fringe contrast, we find that we achieve 4dB of spin squeezing [18], and 3dB of improvement in clock signal-to-noise ratio over the standard quantum limit [14,15]. The contrast loss is not fundamental, and in part simply limited by the detuning and intensity of the light used to stabilize the resonator length. We are currently making modifications to the setup to reduce this technical noise. If successful, the improvement in signal-to-noise ratio should allow us to obtain an improvement over the SQL that matches the observed spin noise reduction of 9dB. If technical noise can be suppressed further, a fundamental limit associated with scattering into free space is set by the optical depth OD of the sample [17], which for our present parameters (OD $\approx 5\times10^3$) would amount to ~18 dB of spin squeezing.

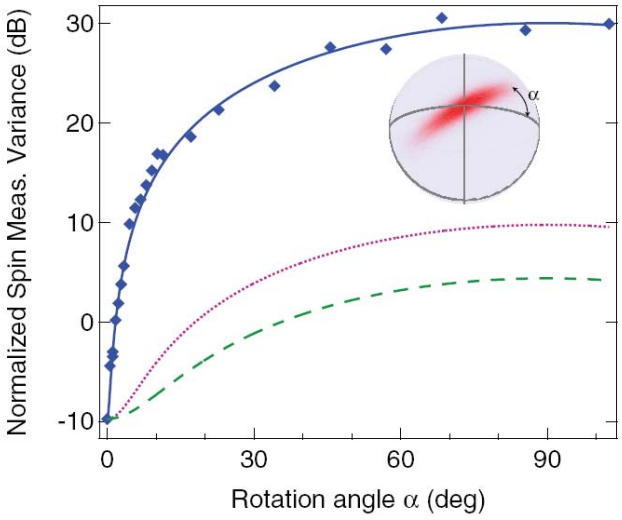

Figure V7. Shape of the squeezed uncertainty region. A rotation about the mean spin vector $\langle \boldsymbol{S} \rangle$ is applied between the first and second spin measurements. The spin noise reduction along z (α=0) below the projection noise limit is accompanied by a substantial spin noise increase in the equatorial plane ($\alpha=\pi/2$). The solid blue line corresponds to an elliptic shape of the uncertainty region. The dotted magenta line would correspond to a state at the Heisenberg limit in the ideal case where the measurement does not reduce the length of the spin vector $|\boldsymbol{S}|$. The dashed green line is the true Heisenberg limit for our measurement, taking into account the reduction of $|\boldsymbol{S}|$.

References

1. M. Saba, T.A. Pasquini, C. Sanner, Y. Shin, W. Ketterle, and D.E. Pritchard, *Continuous measurement of the relative phase of two Bose-Einstein condensates using light scattering*, Science **307** (2005).
2. Y. Shin, G.-B. Jo, M. Saba, T.A. Pasquini, W. Ketterle, and D.E. Pritchard, *Optical Weak Link between Two Spatially Separate Bose-Einstein Condensates*, Phys. Rev. Lett. **95**, 170402 (2005).
3. Y. Shin, C. Sanner, G.-B. Jo, T.A. Pasquini, M. Saba, W. Ketterle, D.E. Pritchard, M. Vengalattore, and M. Prentiss, *Interference of Bose-Einstein Condensates on an Atom Chip*, Phys. Rev. A **72**, 021604(R) (2005).
4. T.A. Pasquini, Y. Shin, C. Sanner, M. Saba, A. Schirotzek, D.E. Pritchard, and W. Ketterle, *Quantum reflection of atoms from a solid surface at normal incidence*, Phys. Rev. Lett. **93**, 223201 (2004).
5. R.G. Scott, A.M. Martin, T.M. Fromhold, and F.W. Sheard, *Anomalous Quantum Reflection of Bose-Einstein Condensates from a Silicon Surface: The Role of Dynamical Excitations*, Phys. Rev. Lett. **95**, 073201 (2005).
6. T.A. Pasquini, M. Saba, G. Jo, Y. Shin, W. Ketterle, D.E. Pritchard, T.A. Savas, and N. Mulders, *Low velocity quantum reflection of Bose-Einstein condensates*, Phys. Rev. Lett. **97**, 093201 (2006).
7. G.-B. Jo, Y. Shin, S. Will, T.A. Pasquini, M. Saba, W. Ketterle, D.E. Pritchard, M. Vengalattore, and M. Prentiss, *Long Phase Coherence Time and Number Squeezing of two Bose-Einstein Condensates on an Atom Chip*, Phys. Rev. Lett. **98**, 030407 (2007).
8. C.A. Christensen, S. Will, M. Saba, G.-B. Jo, Y.Shin, W. Ketterle, and D.E. Pritchard, *Trapping of Ultracold Atoms in a Hollow-core Photonic Crystal Fiber*, Phys. Rev. A **78**, 033429 (2008).
9. G.-B. Jo, J.-H. Choi, C.A. Christensen, T.A. Pasquini, Y.-R. Lee, W. Ketterle, and D.E. Pritchard, *Phase Sensitive Recombination of Two Bose-Einstein Condensates on an Atom Chip*, Phys. Rev. Lett. **98**, 180401 (2007).
10. G.B. Jo, J.H. Choi, C.A. Christensen, Y.R. Lee, T.A. Pasquini, W. Ketterle, and D.E. Pritchard, *Matter-Wave Interferometry with Phase Fluctuating Bose-Einstein Condensates*, Phys. Rev. Lett. **99**, 240406 (2007).
11. PhD Thesis for Saijun Wu at Harvard University 2007
12. PhD Thesis for Pierre Streihl at Harvard University 2007
13. Wu S, Su E, Prentiss M, Demonstration of an area-enclosing guided-atom interferometer for rotation sensing ,Phys. Rev. Lett. 99, 173201 (2007)
14. D. J. Wineland, J. J. Bollinger, W. M. Itano, F. L. Moore, D. J. Heinzen, "Spin squeezing and reduced quantum noise in spectroscopy," Phys. Rev. A **46**, R6797 (1992).
15. D. J. Wineland, J. J. Bollinger, W. M. Itano, D. J. Heinzen, "Squeezed atomic states and projection noise in spectroscopy," Phys. Rev. A **50**, R67 (1994).
16. V. Meyer, M. A. Rowe, D. Kielpinski, C. A. Sackett, W. M. Itano, C. Monroe, and D. J. Wineland, "Experimental Demonstration of Entanglement-Enhanced Rotation Angle Estimation Using Trapped Ions," Phys. Rev. Lett. **86**, 5870-5873 (2001).

17. D. Leibfried, M.D. Barrett, T. Schaetz, J. Britton, J. Chiaverini, W.M. Itano, J.D. Jost, C. Langer, and D. Wineland, “Toward Heisenberg-Limited Spectroscopy with Multiparticle Entangled States," Science **304**, 1476 (2004).
18. M. Kitagawa and M. Ueda, “Squeezed spin states,” Phys. Rev. A **47**, 5138 (1993).
19. A. Kuzmich, N. P. Bigelow, and L. Mandel, “Atomic quantum non-demolition measurements and squeezing,” Europhys. Lett. **42**, 481-486 (1998).